High Performance PMSM Sensorless Drive Based on Stochastic Filtering

S. Bolognani, M. Zigliotto, M. Zordan
Department of Electrical Engineering
University of Padova
Italy
mauroz@dei.unipd.it

Abstract

This paper describes the prototype realisation of a high-performance sensorless Permanent Magnet Synchronous Motor (PMSM) drive. Experimental setup, hardware circuitry and software implementation are described into details; particular emphasis is given to the software control algorithms specifically studied and implemented to increase the overall system performance.

1. Historical Background

Certainly, the realisation of a high-performance sensorless Permanent Magnet Synchronous Motor (PMSM) drive is not a trivial task. Former works on stochastic filtering estimation [1-3], especially those related to extended Kalman filter (EKF), focused on the theoretical aspects, proving by simulation the effectiveness of the solution and preparing the basis for the successive evolution of the research. Unfortunately, the complex matrix calculations, together with the very short control cycle requirement, have curbed the experimental validations, giving rise to a dispute on the cost-to-benefits aspects.

Actually, only the latest drive-oriented digital signal processors (DSP) equipped with embedded or matched peripherals are marking a turning point in sensorless drives.
Their mass-production reduces prices and floating-point operations give the system the accuracy that is a must for EKF convergence.
The available DSP chips are capable of tens of MFLOPs and this absolutely high speed (unusual in conventional drive control systems) let the designer to complete the main algorithm with several software tricks that give the system superior robustness and good dynamic performance.

This paper describes the ultimate results on a laboratory prototype of a EKF-based sensorless PMSM drive. The work takes advantage of previous studies and experiments carried out by the authors in the last six years and it successfully deals with the items that have represented the hardest obstacles in the past, often making the stochastic approach useless. In particular the following features have been successfully implemented:

- enhanced current control, with space vector modulator (SVM) and dead time compensation
- fast EKF initial convergence, regardless to the standstill rotor position;
- improved pull-in and pull-out characteristic;
- on-line tuning of the PM flux linkage.

The paper gives the details of each of them. In the final section, the experimental evidences and final considerations on the application are reported.

2. PMSM Equations and EKF Basics.

Let's assume a stationary orthogonal reference frame α,β fixed to the stator. The two PMSM voltage equations and the two load dynamic equations can be rearranged in a canonical state-space form as follows [4]:

$$\begin{cases} \dfrac{di_\alpha}{dt} = -\dfrac{R}{L} i_\alpha + \omega \dfrac{\Lambda_{mg}}{L} \sin(\vartheta) + \dfrac{u_\alpha}{L} \\ \dfrac{di_\beta}{dt} = -\dfrac{R}{L} i_\beta - \omega \dfrac{\Lambda_{mg}}{L} \cos(\vartheta) + \dfrac{u_\beta}{L} \\ \dfrac{d\omega}{dt} = 0 \\ \dfrac{d\vartheta}{dt} = \omega \end{cases} \quad (1)$$

The motor phase currents i_α and i_β, the electrical speed ω and position ϑ are chosen as system state variables:

$$\mathbf{x} = \begin{bmatrix} i_\alpha & i_\beta & \omega & \vartheta \end{bmatrix}' \quad (2)$$

The phase voltages u_α and u_β represent the components of the input vector **u**, while i_α and i_β form the output vector **y**. With the above

assumptions, the system model can be expressed in the form

$$\begin{cases} \mathbf{x}(t) = \mathbf{f}\big(\mathbf{x}(t), \mathbf{u}(t)\big) + \boldsymbol{\nu}(t) \\ \mathbf{y}(t_k) = \mathbf{h}\big(\mathbf{x}(t_k)\big) + \boldsymbol{\mu}(t_k) \end{cases} \tag{3}$$

where bold characters are used for vectors and matrices, and zero-mean Gaussian noises $\boldsymbol{\nu}(t)$ and $\boldsymbol{\mu}(t)$, whose variance matrices are $\mathbf{Q}$ and $\mathbf{R}$ respectively, account for model and measurement disturbances. The system (3) is then linearised and discretised with time step T_c around the best available state vector $\mathbf{x}_o$ [3]. In the model equations, the moment of inertia J is chosen intentionally very high, and this is the same as neglecting the influence of speed variations within the time step T_c in the model itself.

At time t_k the optimal state estimate $\mathbf{xe}_{k|k}$ and the estimation error covariance matrix $\mathbf{P}_{k|k}$ are obtained through the well-known two-step EKF procedure [2,3]:

Step 1 - *Prediction*

$$\begin{aligned} \mathbf{xe}_{k|k-1} &= \mathbf{xe}_{k-1|k-1} + \Big[\mathbf{f}\big(\mathbf{xe}_{k-1|k-1}\big) + \mathbf{B}\langle \mathbf{u}_{k-1}\rangle\Big] T_c \\ \mathbf{P}_{k|k-1} &= \boldsymbol{\Phi}_{k-1}\mathbf{P}_{k-1|k-1}\boldsymbol{\Phi}'_{k-1} + \mathbf{Q} \end{aligned} \tag{4}$$

Step 2 - *Innovation*

$$\begin{aligned} \mathbf{xe}_{k|k} &= \mathbf{xe}_{k|k-1} + \mathbf{K}_k\Big[\mathbf{y}_k - \mathbf{H}\,\mathbf{xe}_{k|k-1}\Big] \\ \mathbf{P}_{k|k} &= \mathbf{P}_{k|k-1} - \mathbf{K}_k\mathbf{H}\,\mathbf{P}_{k|k-1} \end{aligned} \tag{5}$$

where $\boldsymbol{\Phi}$ is the exponential matrix of the linearised system, that has been approximated by

$$\boldsymbol{\Phi}(t_k, t_{k-1}, \mathbf{x}(t_{k-1})) \cong \mathbf{I} + \mathbf{F}T_c \tag{6}$$

and $\mathbf{F}$, $\mathbf{B}$ and $\mathbf{H}$ are respectively the state, the input and output matrices of the linearised system. The *gain matrix* $\mathbf{K}$ is given by:

$$\mathbf{K}_k = \mathbf{P}_{k|k-1}\mathbf{H}'\Big[\mathbf{H}\,\mathbf{P}_{k|k-1}\mathbf{H}' + \mathbf{R}\Big]^{-1} \tag{7}$$

Covariance matrices $\mathbf{P}$, $\mathbf{Q}$ and $\mathbf{R}$ are symmetric and positive semidefinite, and it has been shown [4] that this property is crucial for a correct EKF convergence. While $\mathbf{Q}$ and $\mathbf{R}$ can be considered constant with light effects on the EKF dynamics [4], $\mathbf{P}$ is updated every control cycle T_c, according to (4) and (5). Rounding errors due to the finite length of the digital word could sum up, and the critical subtraction performed in the innovation step to derive $\mathbf{P}_{k|k}$ could affect the convergence process. This problem has a deep impact in fixed-point DSP implementation. Floating point operations are certainly less affected by rounding and truncating effects, nevertheless better EKF performances have been obtained implementing the so-called *symmetric form*,

$$\begin{aligned} \mathbf{P}_{k|k} = &\Big[\mathbf{I} - \mathbf{K}_k\mathbf{H}_{k-1}\Big]\mathbf{P}_{k|k-1}\Big[\mathbf{I} - \mathbf{K}_k\mathbf{H}_{k-1}\Big]' + \\ &+ \mathbf{K}_k\mathbf{R}\mathbf{K}'_k \end{aligned} \tag{8}$$

instead of the second of (5).

Expression (8) tackles the critical subtraction in (5) and reduces the sensibility to the rounding errors also for the gain matrix $\mathbf{K}$.

3. Experimental Setup

The structure of the full-digital sensorless PMSM drive realised for this paper is reported in Fig.1.

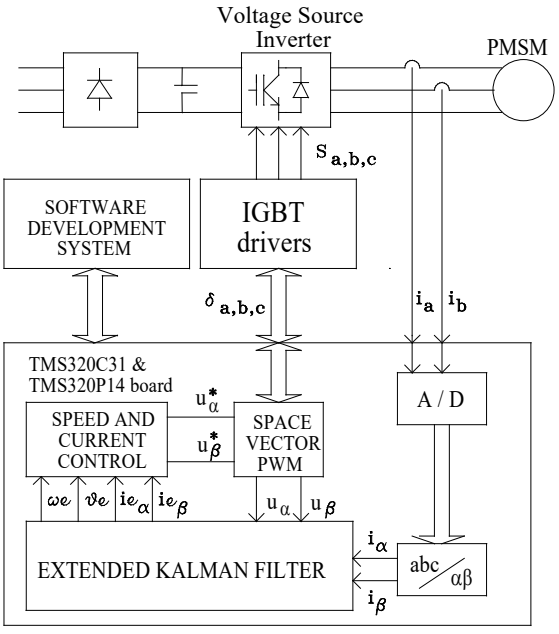

Fig.1 - Experimental Setup

The speed and current estimated values are used to realise two nested control closed loops, whose details will be given later on in the

paper. The EKF algorithm, speed and current control loops, voltage space vector modulation (SVM) timings and dead time compensation have been implemented on a TMS320C31 Floating Point DSP, with 33.3ns instruction cycle. All software procedures are written in C language, optimised for shortest execution time. In particular, matrix calculation have been made explicit beforehand, to exploit the symmetry and the large number of zero elements. Moreover, unconditional branches have been drastically limited, to optimise pipeline flow and reduce DSP instruction cache reload. Digital I/O management and switching pattern generation are handled by a slave Fixed Point TMS320P14 DSP, with 160 ns instruction cycle, featuring six PWM channels, with 80 ns period resolution and 16 individual bit-selectable I/O. Control software routines for the slave processor have been written in Assembly language, for a closer link with the embedded hardware peripherals. Phase currents have been measured by two parallel autocalibrating 16-bit 10 µs A/D converters, while speed reference and DC link bus voltage are measured by two 12-bit 3 µs A/D converters.
The detailed execution times of the different part of the main control interrupt routine have been reported in the following Tab.1.

Tab.1 - Main control task execution times [µs]

Prediction step	16.7
Innovation step	29.6
Current acquisitions and abc/αβ transformation	7
Trigonometric function retrieval, αβ/dq transformation and current control	17.9
dq/αβ and R/P transformations	5.8
SVM algorithm	7.9
Dead time compensation	3.1
Master-slave communication	2.8
Save/restore status	7.3

The total execution time is of 98.1 µs. Considering a safe DSP load coefficient of 80%, a control period T_c=125 µs has been selected, that is a 8 KHz switching frequency.

4. Current Control and dead time Compensation

The current control plays a crucial rule in the overall behaviour of the drive. The push towards full-digital implementation gives an extra-challenge for the designer, especially if performances similar to those of analog schemes are pursued. Due to the inherent simplicity of the regulator tuning and the zero steady-state error feature, two PI control loops have been implemented in a synchronous rotating d-q reference frame. Feedforward emf compensation and loop decoupling have been implemented as well. The complete current control scheme is reported in Fig.2.

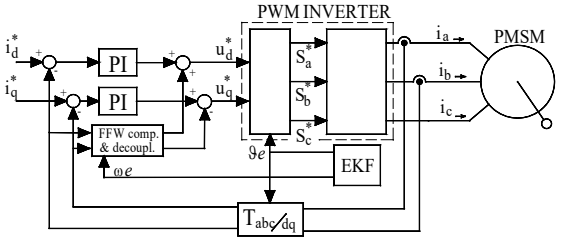

Fig.2 - Current control scheme

With a control period of 125 µs, and an accurate tuning of the PI regulators, a bandwidth of about 850 Hz has been measured. In the proposed implementation, the measurement of the voltage applied to the motor is no longer required, and reference SVM signal are used instead. It has been found that this approximation is not effective at low speed unless a proper dead time compensation is performed. In conventional algorithms [4] the sign of voltage compensation is decided by the sign of phase currents, that have to be properly detected at each modulation cycle. Particular care has been paid to current acquisition. Synchronous sampling reduces the modulation noise but external hardware filtering has been necessary to reject high frequency noise (mainly due to the sharp IGBT commutation edges) that strongly deteriorates the A/D acquisitions. Low-pass first-order filters with 6 KHz cut-off frequency have shown good performances. Nonetheless, they introduce an unwanted delay that can be mitigated by a current software post-processing:

$$
\begin{aligned}
i_a &= i_a + k(i_c - i_b) \\
i_b &= i_b + k(i_a - i_c) \\
i_c &= i_c + k(i_b - i_a)
\end{aligned} \qquad (9)
$$

that corresponds to add a lead component to each phase current. The entity of the compensation depends on the value of k, that has the same sign of motor speed and an amplitude that linearly decreases with speed itself. Hereafter low speed α–β voltages (directly obtained from phase voltages measured on motor terminals and filtered by a first order, 100 Hz cut-off frequency filter) are shown.

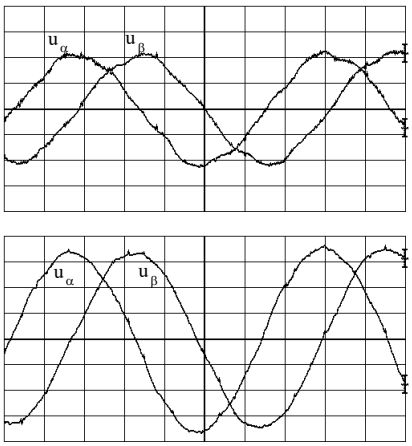

y axis: 3.2 V/div.; *x* axis: 10 ms/div.
Fig.3 - u_α, u_β without (upper) and with (lower) proposed DT compensation

As expected, the amplitude is corrected and a good sinusoidal shape is obtained.

5. Start-up Procedure

In the proposed drive, a dedicated algorithm ensures that the speed and position estimation operates properly at start-up, even if the actual rotor initial position is unknown and different from the initial value assumed by the algorithm. This feature aims to overcome some drawbacks of other estimation techniques already developed, for example those that force the rotor in a known home position [2].
It is easy to recognise that motor model voltage equations formally admit two solutions, the correct one (ω, ϑ) and the wrong one (-ω, ϑ+π). As found in [3], the wrong solution is maintained by the innovation step that continuously updates the estimate, compensating for the gap between the actual and predicted currents and voltages. Fig.4 reports an experimental evidence of the misconvergence.

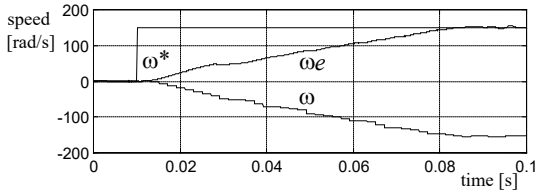

Fig.4 - EKF misconvergence at start-up

Estimated speed ω*e* coincides with dϑ*e*/dt only if the EKF is converged to the correct couple (ω,ϑ). Whether a misconvergence should be detected, both a skip of π is forced on the rotor position and the estimated speed is reversed. The effective result of this correction procedure is reported in Fig.5.

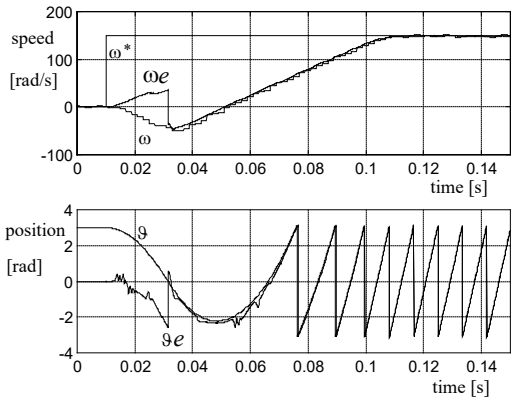

Fig.5 - Proposed correction at start-up

The possible start-up misconvergence is checked after the EKF convergence (to either solution), that can be sensed from the evolution of the position error variance element P_{44} in the covariance matrix P, which is normally large during transients and rather small after EKF convergence. Only when that element goes below a certain threshold the estimates are reliable and the correction is performed.

6. Stall Condition Avoidance

Many practical applications require the drive ability of a loaded start-up. If the initial electrical position error is close to ±π/2 the

EKF convergence time increases considerably. The delay arises because a ±π/2 position error causes the swapping of the flux and torque current components, and under FOC operation this results in a null torque production. The rotor lies in an unstable equilibrium point (*stall condition*). An experimental evidence, from the laboratory prototype, is reported in Fig.6.

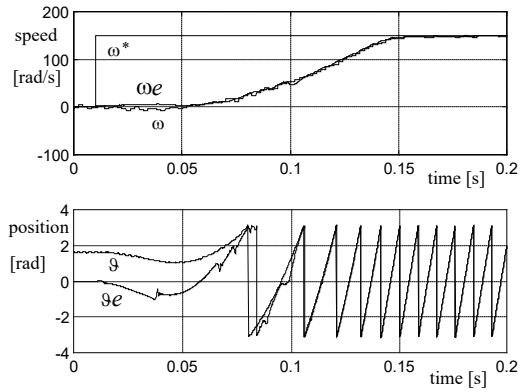

Fig.6 - Delay caused by stall condition

If the static torque is remarkably high so to prevent any movement, the rotor is locked and the EKF estimates diverge. There exist different ways to deal with the stall condition. In this work, the simple i_d *transient current pulse* approach studied in [5] has been implemented. Briefly, a transient flux-producing current component is initially forced, for example an exponentially decaying waveform. It gives active torque if initial ±π/2 position mismatching is encountered. Some trial-and-error experiments have suggested that a satisfactory d-current reference is given by

$$i_d^* = \frac{I_N}{2} e^{-t/4\tau_a} \qquad (10)$$

where I_N is the rated motor current and τ_a is the motor electrical time constant. The improvements in the drive behaviour are reported in Fig.7, obtained under the same initial load condition.

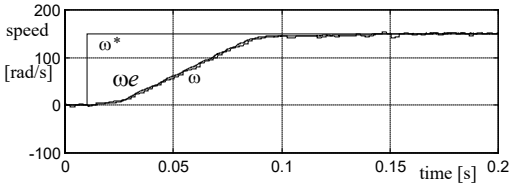

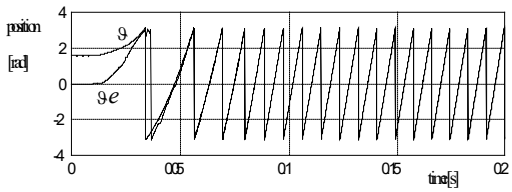

Fig.7 - Start-up with i_d pulse

It is evident the faster speed convergence and the smart position estimate behaviour.

7. Electrical Parameters On-line Tuning

Experimental tests have shown that the proposed EKF algorithm is robust against mechanical parameter variations. Conversely, the sensibility to electrical parameters uncertainty represents an heavy disadvantage. In particular, EKF estimate is very sensitive to the PM flux linkage model error, that gives as much speed estimate inaccuracy [6].
The proposed closed-loop on-line tuning procedure is sketched in Fig.8.

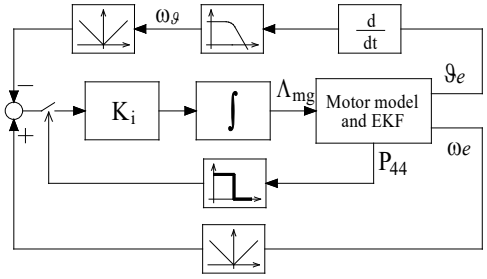

Fig.8 - PM flux-linkage on-line tuning scheme

The time derivative of the estimated position coincides with the actual speed but due to superimposed noise, its use as speed feeback is unpractical. It is fairly better to compare it with the estimated speed ω*e*, ascribing the error to a flux linkage imprecision. The integral of the error is used to update the Λ_{mg} model value, until a zero steady-state error is achieved. As usual, the procedure is triggered after a successful convergence, detected by monitoring the evolution of the P_{44} element.
In Fig.9 an intentionally wrong value $\Lambda_{mg} = 80$ mVs is initially given to the EKF algorithm. The proposed correction algorithm is triggered after 0.5 s, and it slowly update the flux-linkage value. With the same dynamics, the actual speed is driven to its correct value.

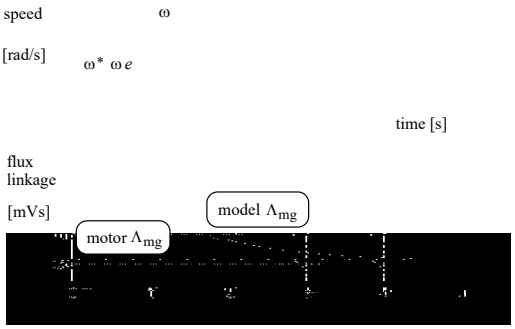

Fig.9 - On-line flux linkage correction

8. Pull-in and pull-out Characteristics

Any PMSM sensorless drive realisation is characterised by its ability to deliver the rated torque over the widest speed range. This is readily get measuring the *pull-out curve* of the drive, as shown in Fig.10.

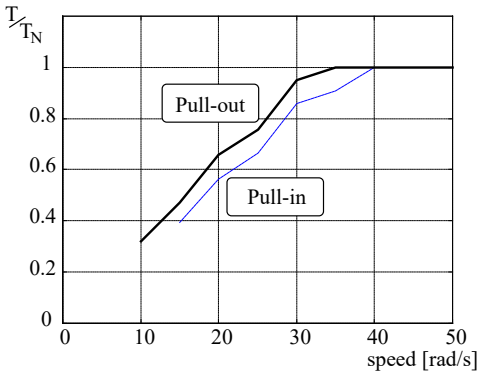

Fig.10 - Pull-out and pull-in curves

Once started, the proposed PMSM drive is able to deliver the nominal torque from the nominal speed (419 rad/s) down to 35 rad/s, that is a speed ratio of 1:12. Then the torque-delivery capability decreases to 30% at 10 rad/s. Beyond that speed reference, noise and inaccuracies in measured quantities inhibits proper EKF convergence. The ability of the drive to start in a loaded condition, under a speed step reference, has also been investigated. The relative *pull-in curve* is also presented in Fig.10, with a dashed thin line. It is shown that the minimum full-load start-up speed is 40 rad/s. Finally, the speed loop dynamics has been tested on the laboratory prototype. The bandwidth was of about 20 Hz, measured at 100 rad/s with the small-step response method.

Acknowledgements

The authors gratefully acknowledge Texas Instruments ELITE research program for the precious technical and financial support during the experimental stage of the work.

Conclusions

The paper describes the prototype realisation of a full-digital DSP-based PMSM sensorless drive. The achieved results smooth the way for the industrialisation and commercialisation of the drive, that will be the next step to be taken.

References

[1] L. A. Jones and J. H. Lang, "A state observer for permanent-magnet synchronous motor", IEEE Trans. on Ind. Electr., vol. 36, no. 3, 1989, pp. 374-382.

[2] R. Dhaouadi and N. Mohan, "Application of stochastic filtering to a permanent magnet synchronous motor-drive system without electro-mechanical sensors", Proc. of ICEM 90, pp. 1225-1230.

[3] S. Bolognani, R. Oboe and M. Zigliotto, "DSP-based Extended Kalman Filter Estimation of Speed and Rotor Position of a PM Synchronous Motor", Proc. IEEE-IECON, 1994, vol. 3, pp. 2097-2102

[4] M.Zordan, "Innovative Controls for PMSM Drives" PhD Thesis, University of Padova, Italy, 1998 (*in italian*).

[5] S. Bolognani, M. Zigliotto and M. Zordan, "Rotor Position Detection for Sensorless PM Synchronous Motor Drives", 8th Int. Power Electronics & Motion Control Conference, PEMC'98, pp. 8.83-8.88.

[6] S.Bolognani, M. Zigliotto and K. Unterkofler, "On-line Parameters Commissioning in Sensorless PMSM Drives", Proc. International Symposium on Industrial Electronics, ISIE 97, vol. 2, pp. 480-484

[7] Hen-Geul Yeh, "Real-time implementation of a narrow-band Kalman filter with a floating-point processor DSP32", 1990 IEEE Trans. on Industrial Electronics IE-37, pp.13-18.

Appendix - PMSM data

Nominal torque	2.8 Nm
Nominal speed	420 rad/s
PM flux linkage	0.066 Vs
Phase resistance	1.5 Ω
Phase inductance	3.5 mH
Pole pairs	4